PROTEINS: Structure, Function, and Genetics 41:460–474 (2000)

Backbone Dynamics of Barstar: A ^{15}N NMR Relaxation Study

Sarata C. Sahu,[1] Abani K. Bhuyan,[2–4]* Ananya Majumdar,[1] and Jayant B. Udgaonkar[4]*
[1]*Department of Chemical Sciences, Tata Institute of Fundamental Research, Mumbai, India*
[2]*Centre for Biochemical Technology (CSIR), Delhi University Campus, Delhi, India*
[3]*Jawaharlal Nehru Centre for Advanced Scientific Research, Jakkur, Bangalore, India*
[4]*National Centre for Biological Sciences, Tata Institute of Fundamental Research, GKVK, Bangalore, India*

ABSTRACT **Backbone dynamics of uniformly ^{15}N-labeled barstar have been studied at 32°C, pH 6.7, by using ^{15}N relaxation data obtained from proton-detected 2D {^{1}H}-^{15}N NMR spectroscopy. ^{15}N spin-lattice relaxation rate constants (R_1), spin-spin relaxation rate constants (R_2), and steady-state heteronuclear {^{1}H}-^{15}N NOEs have been determined for 69 of the 86 (excluding two prolines and the N-terminal residue) backbone amide ^{15}N at a magnetic field strength of 14.1 Tesla. The primary relaxation data have been analyzed by using the model-free formalism of molecular dynamics, using both isotropic and axially symmetric diffusion of the molecule, to determine the overall rotational correlation time (τ_m), the generalized order parameter (S^2), the effective correlation time for internal motions (τ_e), and NH exchange broadening contributions (R_{ex}) for each residue. As per the axially symmetric diffusion, the ratio of diffusion rates about the unique and perpendicular axes ($D_\parallel/D_\perp$) is 0.82 ± 0.03. The two results have only marginal differences. The relaxation data have also been used to map reduced spectral densities for the NH vectors of these residues at three frequencies: 0, ω_H , and ω_N, where $\omega_{H,N}$ are proton and nitrogen Larmor frequencies. The value of τ_m obtained from model-free analysis of the relaxation data is 5.2 ns. The reduced spectral density analysis, however, yields a value of 5.7 ns. The τ_m determined here is different from that calculated previously from time-resolved fluorescence data (4.1 ns). The order parameter ranges from 0.68 to 0.98, with an average value of 0.85 ± 0.02. A comparison of the order parameters with the X-ray B-factors for the backbone nitrogens of wild-type barstar does not show any considerable correlation. Model-free analysis of the relaxation data for seven residues required the inclusion of an exchange broadening term, the magnitude of which ranges from 2 to 9.1 s^{-1}, indicating the presence of conformational averaging motions only for a small subset of residues. Proteins 2000;41:460–474.** © 2000 Wiley-Liss, Inc.

Key words: nuclear spin relaxation; backbone dynamics by NMR

INTRODUCTION

Barstar is an 89 amino acid protein produced intracellularly by *Bacillus amyloliquefaciens* and acts to inhibit barnase, the ribonuclease secreted by the same bacterium.[1] Starting from Hartley and Smeaton's seminal work[2] barstar has been regarded as an important protein for a number of reasons. (a) The 1:1 interaction between barstar and barnase has been known to be one of the most high-affinity protein-protein interactions with a K_d of 2×10^{-14} M.[2,3] This serves as a model system to study various physical and chemical determinants of protein-protein interactions. Indeed, the complex of barstar and barnase has been examined by both X-ray crystallography[4] and NMR spectroscopy.[5] (b) Barstar has been used in neutralizing the cytotoxic effects of heterologous expression of barnase in genetic engineering applications.[6,7] (c) Recently, barstar has been more extensively used as a model protein to study polypeptide folding and stability and the effects of structure on backbone amide hydrogen exchange (see, e.g., Refs. 3, 8, and 9).

These considerations have aroused interest in the atomic structure of the protein. Lubienski et al.[7,10] have assigned the ^{13}C, ^{15}N, and ^{1}H resonances in the NMR spectra of the wild-type protein and reported the restrained minimized mean structure in solution. Recently, Wong et al.[11] described the NMR solution structure of the C40/82A mutant of barstar. The structures of the wild-type and the mutant protein have been found to be superimposable. A model diagram of the wild-type barstar 1BTA[7] is presented in Figure 1. It is composed of three α-helices packed against a three-stranded parallel β-sheet and a small helix. This

Abbreviations: NMR, nuclear magnetic resonance; 2D, two-dimensional; R_1(= $1/T_1$), spin-lattice relaxation rate; R_2 (= $1/T_2$), spin-spin relaxation rate; NOE, nuclear Overhauser effect; S^2, generalized order parameter; τ_m, rotational correlation time; τ_e, effective correlation time for internal motions; R_{ex}, exchange contribution to line shape; ω, Larmor frequency; D, diffusion constant; CSA, chemical shift anisotropy; C40/82A, double mutant of barstar with Cys 40 and Cys 82 both changed to Ala; RMSD, root mean square distance.

Grant sponsor: Tata Institute of Fundamental Research; Grant sponsor: Department of Biotechnology, Government of India.

The Supplementary Material referred to in this article can be found at http://www.interscience.wiley.com/jpages/0887-3585/suppmat/41_4/v41_4.460.html

*Correspondence to: Abani K. Bhuyan, Centre for Biochemical Technology (CSIR), Delhi University Campus, Mall Road, Delhi, India 110007. E-mail: abani@cbt.res.in or Jayant B. Udgaonkar, National Centre for Biological Sciences, Tata Institute of Fundamental Research, GKVK, Bangalore, India. E-mail: jayant@ncbs.res.in

Received 4 June 1999; Accepted 13 July 2000

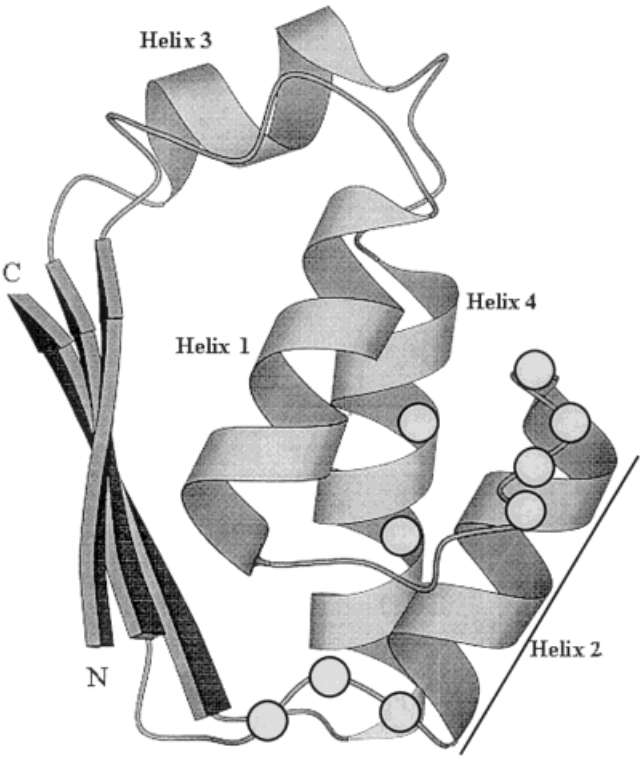

Fig. 1. A Molscript[63] ribbon diagram of barstar based on NMR solution structure.[7] All residues forming helix 2 and the ones shown by circles are involved in barnase binding. The highlighted residues preceding helix 2 are Tyr 29, Tyr 30, Glu 31, and E 32. Residues 33–43 form helix 2. Trp 44, Val 45, and Glu 46 form part of the turn following helix 2, and Gln 73 and Glu 76 are from helix 4.

small helix is positioned between the second β-strand and the third major α-helix. The X-ray structure of the barstar-barnase complex has implicated residues 29–46, and 73 and 76 of barstar in making contacts with barnase.[4] In this article these residues will be referred to as barnase-binding residues.

Because wild-type barstar with the two cysteines, Cys 40 and Cys 82, was suspected to aggregate, and because the heterogeneity of the oxidation state appeared to hamper X-ray studies, Fersht and colleagues chose to use C40/82A for a number of folding and structural studies. While the present work on the backbone dynamics of the wild-type barstar was in progress, Wong et al.[11] reported the solution structure and backbone mobility of C40/82A. Both of these studies have used ^{15}N relaxation measurements using heteronuclear {^1H}-^{15}N spectroscopy to study backbone dynamics by extended model-free calculations,[12–14] and reduced spectral density mapping.[15–18] Thus, in addition to reporting on the backbone dynamics of wild-type barstar, the availability of dynamics data on the C40/82A mutant provides an opportunity to compare the present results with those for the mutant. We have analyzed the data by using both axially symmetric and isotropic molecular diffusion models. The results presented in the text are for the axially symmetric molecular diffusion model; however, the results obtained for both diffusion models are given in the supplementary material (http://www.interscience.wiley.com/jpages/0887-3585/suppmat/index.html).

In the present study, the overall molecular tumbling correlation time of wild-type barstar has been determined to be 5.2 ns from the extended model-free analysis and 5.7 ns from reduced spectral density mapping. The extended model-free analysis shows that 42 backbone NH vectors exhibit fast internal motion, and 7 NH vectors, of which 4 belong to the barnase-binding loop and 3 other contiguous residues define the loop between the third and the fourth helix, have exchange contribution to R_2. In the spectral density map, 15 residues are identified with slower internal motions. The map also indicates higher mobility NH vectors in the N- and C-termini of the polypeptide. We have also compared the X-ray B-factors of the backbone nitrogens with the order parameters and have not found any considerable correlation. The present results are not fully comparable with those for the mutant, C40/82A. The dynamics of the latter, relative to those of the wild-type protein, appear to be characterized by a somewhat rigid backbone and by slow conformational exchanging motions spread over many residues. These results are important because they tend to indicate that the backbone dynamics of the wild-type and the mutant protein are not quite similar, even though the solution structures of the two proteins have been reported to be superimposable.[11]

MATERIALS, METHODS, AND THEORETICAL CONSIDERATIONS

Culture Growth and Protein Purification

The plasmid encoding the barstar gene (pMT316) was transformed into *E. coli* strain MM294. ^{15}N isotopically enriched barstar was produced by using M9 minimal medium prepared with $^{15}NH_4Cl$ (1 g/L) as the sole source of nitrogen. Cells were grown at 37°C for about 20 h. After 8 h of inoculation, protein expression was induced by adding IPTG to a final concentration of 0.1 mM. The procedure for purification of the protein was described previously.[19] The yield of uniformly ^{15}N-labeled barstar was approximately 5 mg/L of culture.

Sample Preparation and NMR Spectroscopy

For NMR experiments, 600 μL of 1 mM ^{15}N-enriched barstar was prepared in 20 mM sodium phosphate buffer, pH 6.7, containing 15% D_2O. All NMR experiments were performed at 32°C on a Varian Unity plus spectrometer operating at a ^1H frequency of 600.051 MHz, equipped with a Performa II pulsed field gradient unit and an actively shielded triple resonance z-gradient probe. Relaxation measurements were performed by using inversion recovery for T_1,[20] Carr-Purcell-Meiboom-Gill sequence for T_2,[21] and steady-state ^1H-^{15}N NOE[22] using the sequences devised by Farrow et al.,[23] which used pulse field gradients for coherence transfer pathway selection combined with sensitivity enhancement.[24,25] Quadrature detection along the indirectly detected dimension was achieved via the States-TPPI method.[26] T_1 and T_2 spectra were recorded as 90 × 2,048

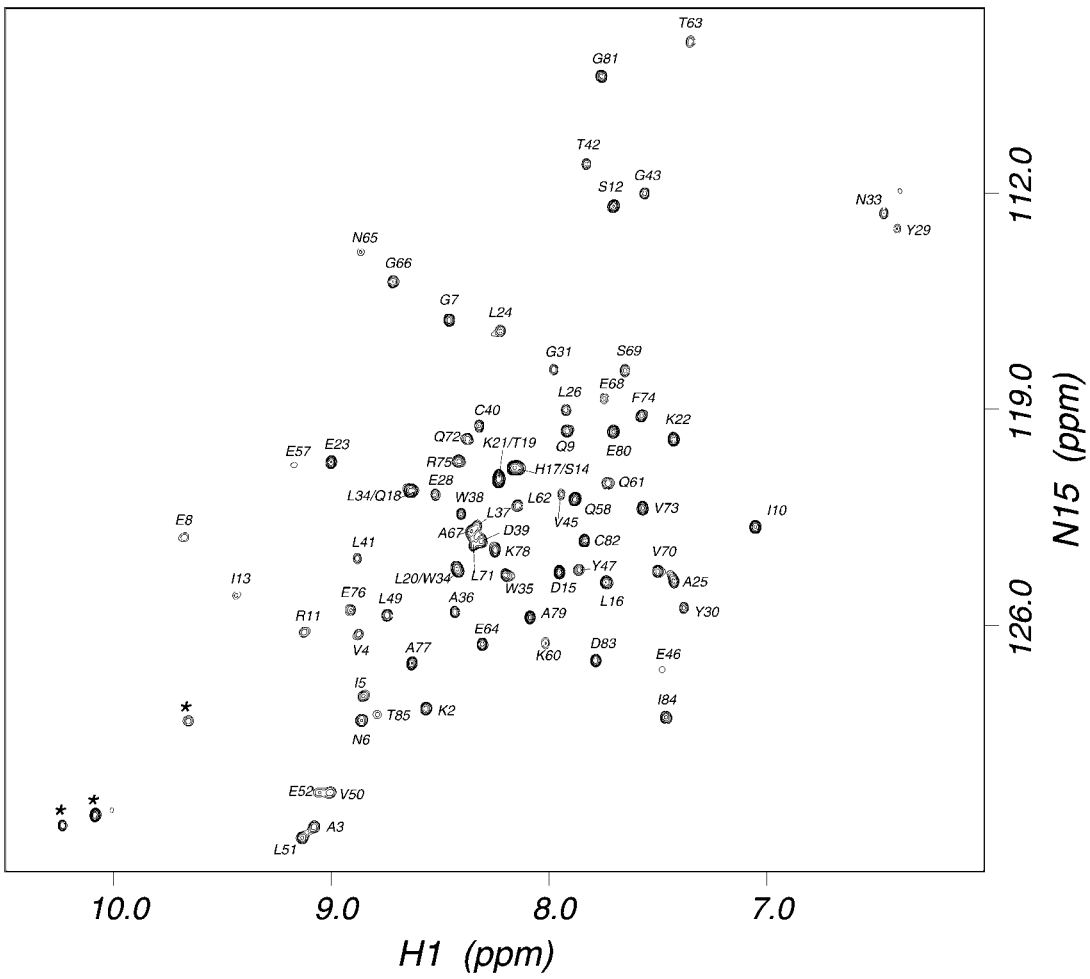

Fig. 2. A portion of the ^{1}H-^{15}N HSQC 2D NMR spectrum of barstar at pH 6.7, 32°C. The peaks marked * are from side-chain indole ^{15}N-^{1}H correlations and are excluded from analysis.

complex matrices with 16 scans per complex t_1 point and spectral widths of 2,000 and 8,500 Hz along the ω_1 and ω_2 dimensions, respectively. A recycle delay of 1.5 s (including the acquisition time) was used for T_1 and T_2 measurements. For R_1 measurement, spectra were recorded with eight inversion recovery delays in the range from 36 to 1,296 ms, and for R_2, spectra were recorded at seven CPMG delays in the range from 15 to 191 ms. The spectra were duplicated at three different time points for each measurement as indicated by ×2 below. The eight inversion recovery delays are as follows: 36 ms, 77 ms (×2), 178 ms, 296 ms (×2), 397 ms, 598 ms, 799 ms (×2), and 1,296 ms. ^{1}H 180° pulses were inserted during the inversion recovery times to eliminate the effects of cross-relaxation time as described previously.[27–29] The seven CPMG delays for R_2 measurement were 15 ms (×2), 31 ms, 46 (×2) ms, 78 ms, 115 (×2) ms, 138 ms, and 191 ms. {^{1}H}-^{15}N NOE spectra of 80 × 2,048 complex matrices with 48 scans for each complex t_1 point were recorded with and without proton saturation during relaxation delay. NOE experiments were duplicated to establish the error in measurement. Spectral widths along the ω_1 and ω_2 dimensions were the same as used in T_1 and T_2 measurements. A recycle delay of 5 s was used for the spectrum recorded in the absence of proton saturation, whereas a 2-s recycle delay followed by a 3-s period of proton saturation was used with the NOE experiment. ^{1}H saturation was achieved by the use of 120° ^{1}H pulses at 5-ms intervals.[30]

Data Processing

All spectra were processed by using FELIX 2.30 (Biosym Technologies). To improve resolution, spectra were linear-predicted by twice the number of acquired points along ω_1 dimension before Fourier transformation. All spectra were zero-filled to 1,024 complex points along ω_1 and 4,096 complex points along ω_2. Resolution enhancement was achieved by applying a Lorentz-Gauss window along ω_2 and a 60°-shifted square sine bell function along ω_1. The final size of the matrices were 2,048(ω_2) × 1,024(ω_1). Most of the peaks were well resolved for peak height measurements (shown in Fig. 2), and peak height measurement is more reliable.[31]

Determination of ^{15}N Relaxation Parameters (R_1, R_2, and NOE)

Intensities (in arbitrary units) for the amide ^{15}N-^{1}H cross peaks were determined by measuring height of the peaks using FELIX software. Uncertainty in the peak height was measured from the duplicate spectra. After obtaining peak heights and their errors, the above time series can be fitted to a single exponential decay function

$$I(t) = A + Be^{-R_{1,2}t} \tag{1}$$

to extract R_1 and R_2, where $I(t)$ is the intensity (obtained from peak height measurements) at recovery delay t (ms) used for measurements of R_1 and R_2 . $A + B$ is the intensity at time $t = 0$, and A is the steady-state value that is the intensity at $t = \infty$. Errors in R_1 and R_2 were estimated as standard errors in R_1 and R_2 from the Lovenberg-Marquardt fitting routine. The errors could also be determined by generating Gaussian random distributions of the peak intensities and repeating the fits many times. Given the good sensitivity of experiments, the errors determined with and without the use of Monte Carlo simulations are not significantly different.

The {^{1}H}-^{15}N heteronuclear NOE was calculated from the equation:

$$NOE = \frac{I_{sat}}{I_{eq}} \tag{2}$$

where I_{sat} and I_{eq} are the intensities of a peak in the spectra collected with and without proton saturation, respectively. Next, two duplicate spectra were analyzed in an identical manner (i.e., Eq. 2) to derive uncertainty of measurements.

Model-Free Analysis

The major sources of relaxation for amide ^{15}N nuclear spins in proteins are dipolar coupling with the attached proton and anisotropy of the ^{15}N chemical shift. The movement of the NH bond axis is characterized by the spectral density function $J(\omega)$, which is related to three parameters that describe the relaxation of the ^{15}N spin: the longitudinal relaxation rate (R_1), the transverse relaxation rate (R_2), and the steady-state NOE enhancement (NOE).[32]

$$R_1 = \frac{1}{4} d^2\{J(\omega_H - \omega_N) + 3J(\omega_N) + 6J(\omega_H + \omega_N)\} + c^2 J(\omega_N) \tag{3}$$

$$R_2 = \frac{1}{8} d^2\{4J(0) + J(\omega_H - \omega_N) + 3J(\omega_N) + 6J(\omega_H) + 6J(\omega_H + \omega_N)\} + \frac{c^2}{6}\{4J(0) + 3J(\omega_N)\} + R_{ex} \tag{4}$$

$$NOE = \frac{d^2}{4R_1} \cdot \frac{\gamma_H}{\gamma_N}\{6J(\omega_H + \omega_N) - J(\omega_H - \omega_N)\} + 1 \tag{5}$$

where

$$d = \frac{\mu_0}{4\pi} \gamma_H \gamma_N \frac{h}{2\pi} (\bar{r_{NH}^3}) \tag{6}$$

$$c = \omega_N(\sigma_\parallel - \sigma_\perp)/\sqrt{3} \tag{7}$$

where μ_0 is the permeability of the free space, γ_H and γ_N are the gyromagnetic ratios of ^{1}H and ^{15}N (2.6752×10^8 and -2.712×10^7 rad s^{-1} T^{-1}, respectively); ω_H and ω_N are the Larmor frequencies of ^{1}H and ^{15}N, respectively, r_{NH} is the N-H bond length (taken here to be 1.02 Å), and $J(\omega_i)$ are the spectral densities at the angular frequencies ω_i. An axially symmetric chemical shift tensor has been assumed for ^{15}N with $\sigma_\parallel - \sigma_\perp = -160$ ppm.[33] R_{ex} has been included in Eq. 4 to accommodate chemical exchange and other pseudo-first-order processes that contribute to the decay of transverse magnetization.[34] The R_{ex} term in Eq. 4 represents line broadening due to chemical exchange and/or conformational averaging on a timescale slower than the overall rotational correlation time, τ_m.

The amplitudes and effective correlation times of the internal motions of protein are determined from the relaxation data by using the model-free formalism pioneered by Lipari and Szabo[12,13] and extended by Clore et al.[14,35] In this analysis, the spectral density function, $J(\omega)$, is modeled differently depending on whether the rotational diffusion tensor is isotropic or anisotropic. In the former case, when the internal motions of the NH bond occur on two fast but significantly different timescales so that they are characterized by two effective correlation times, τ_f and τ_s, with $\tau_f << \tau_s << \tau_m$,[14]

$$J(\omega) = \frac{2}{5}\left[\frac{S^2\tau_m}{1 + (\omega\tau_m)^2} + \frac{(1 - S_f^2)\tau_f'}{1 + (\omega\tau_f')^2} + \frac{(S_f^2 - S^2)\tau_s'}{1 + (\omega\tau_s')^2}\right] \tag{8}$$

in which,

$$\frac{1}{\tau_f'} = \frac{1}{\tau_f} + \frac{1}{\tau_m} \tag{9}$$

$$\frac{1}{\tau_s'} = \frac{1}{\tau_s} + \frac{1}{\tau_m} \tag{10}$$

$S^2 = S_f^2 S_s^2$ is the square of the generalized order parameter characterizing the amplitude of internal motions of each NH bond, and S_f^2 and S_s^2 are the squares of the order parameters for the internal motions on the fast and slower time scales, respectively. The model-free spectral density function in Eq. 8 assumes that the overall tumbling motion of the molecule is isotropic. Motions represented by the generalized order parameter will be referred to as dynamics on the ps to ns timescale. The order parameter specifies the degree of spatial restriction of the NH bond; $S^2 = 1$ for completely restricted motion, and $S^2 = 0$ for completely free motion. S^2 can also have a value of zero when the NH bond vector is static and points along the magic angle with respect to the principal diffusion axis.

For the corresponding model-free expressions for a system that experiences anisotropic rotational diffusion, more complicated expressions have been described.[36–38] However, in the case of axially symmetric tensor, simplification occurs, and the spectral density function is approxi-

TABLE I. Model-Free Spectral Density Functions Used for Relaxation Data Analysis

Model	Spectral density functions	Optimized parameters
1	$J(\omega) = \frac{2}{5}\left[S^2 \sum_{k=1}^{3} \frac{A_k\tau_k}{1+(\omega\tau_k)^2}\right]$	τ_m, S^2
2	$J(\omega) = \frac{2}{5}\left[S^2 \sum_{k=1}^{3} \frac{A_k\tau_k}{1+(\omega\tau_k)^2} + \frac{(1-S^2)\tau}{1+(\omega\tau)^2}\right]$	τ_m, S^2, τ_e
3	$J(\omega) = \frac{2}{5}\left[S^2 \sum_{k=1}^{3} \frac{A_k\tau_k}{1+(\omega\tau_k)^2}\right] + R_{ex}$	τ_m, S^2, R_{ex}
4	$J(\omega) = \frac{2}{5}\left[S^2 \sum_{k=1}^{3} \frac{A_k\tau_k}{1+(\omega\tau_k)^2} + \frac{(1-S^2)\tau}{1+(\omega\tau)^2}\right] + R_{ex}$	$\tau_m, S^2, \tau_e, R_{ex}$

mated for the situations where the internal motions are much faster than overall tumbling rate as:[37]

$$J(\omega) = \frac{2}{5}\left[S^2 \sum_{k=1}^{3} \frac{A_k\tau_k}{1+(\omega\tau_k)^2} + \frac{(1-S^2)\tau}{1+(\omega\tau)^2}\right] \qquad (11)$$

where $A_1 = (1.5\cos^2\alpha - 0.5)^2, A_2 = 3\sin^2\alpha\cos^2\alpha$ and $A_3 = 0.75\sin^4\alpha$. α is the angle between the NH bond vector and the unique axis of the principal frame of the diffusion tensor, $\tau_1 = (6D_\perp)^{-1}$, $\tau_2 = (D_\parallel + 5D_\perp)^{-1}$, $\tau_3 = (4D_\parallel + 2D_\perp)^{-1}$, and $\tau^{-1} = 6D + \tau_e^{-1}$. D is the isotropic diffusion constant, $D_\parallel$ and $D_\perp$ are the components of the diffusional tensor parallel and perpendicular to the principal axis of the axial symmetry, respectively. The isotropic correlation time, τ_m, is related to D by the equation: $\tau_m = (6D)^{-1}$. We have conducted the analysis of the relaxation data by using both approaches.

Dynamic Model Selection and Parameter Estimation

For selection of dynamic model describing internal motion in a residue-specific manner, and to estimate the involved parameters for a model, the numerical optimization procedure of Mandel et al.[39] was used. In this exercise, the spectral densities for the isotropic and axially symmetric diffusion tensors would be of course different. The actual spectral density functions for different dynamic models along with the parameters optimized in the case of axially symmetric diffusion of the molecule are given in Table I. The expression for $J(\omega)$ in each model contains τ_m and not more than three additional internal motional parameters. In the first stage, the best model for a residue was selected by fitting the experimental data to the different models separately, and the one with the minimum number of parameters was preferred. After selecting the best model in this manner, τ_m was optimized along with the other model parameters again by using the grid search method. All optimization involved minimization of the χ^2 function:[39]

$$\chi^2 = \sum_i^n \Gamma_i = \sum_i^n \sum_j^{m_i} (E_{ij} - S_{ij})^2/\sigma_{ij}^2 \qquad (12)$$

where the index i refers to an amide ^{15}N site with n being the total number of sites, and Γ_i is the sum-squared error for site i. m_j represents the number of experimentally determined relaxation parameters for the ith site. E_{ij}, S_{ij}, and σ_{ij}, respectively, are experimental relaxation parameters, simulated relaxation parameters, and the experimental uncertainty in the jth relaxation parameter.

The model calculations were performed by using the program Model-free (version 4.1) provided by Dr. Arthur G. Palmer. To determine random error in the model-free parameters arising from experimental uncertainties, 500 simulated data sets were generated by Monte Carlo simulation, assuming that the standard error in the measured relaxation parameters follow Gaussian distributions. The errors in other parameters (e.g., $D_\parallel/D_\perp$, θ, and ϕ) were also estimated from Monte Carlo simulation.

Reduced Spectral Density Mapping

The model-free approach of analyzing the relaxation data assumes that the spectral density function is a sum of two Lorentzian functions containing S^2, τ_m, and τ_e.[12–14] Peng and Wagner[15,16] described the calculation of power spectral density functions by the use of six ^1H and ^{15}N relaxation rates. The analysis is independent of any form of time dependence of the autocorrelation function, nor does it require any specific form of the rotational diffusion tensor of the molecule. More recent descriptions of reduced spectral density mapping use only three ^{15}N relaxation parameters,[40–45] and provides a convenient method to obtain protein motional information with the assumption that at high frequencies, the spectral density functions: $J(\omega_H) \approx J(\omega_H + \omega_N) \approx J(\omega_H - \omega_N)$. We adopted the procedure described in Lefèvre et al.[18] to first calculate the spectral densities $J(0)$, $J(\omega_N)$, and $J(\omega_H)$, and then examine the linear correlation between $J(0)$ and $J(\omega_N)$, and $J(0)$ and $J(\omega_H)$. By using the above approximation $J(0)$, $J(\omega_N)$, and $J(\omega_H)$ can be expressed in the ^{15}N transverse (R_2) and longitudinal (R_1) relaxation rates and heteronuclear {^1H-^{15}N} NOEs.

$$J(0) = \frac{3}{2(3d' + c')}\left[-\frac{1}{2}R_1 + R_2 - \frac{3}{5}R_{noe}\right] \qquad (13)$$

$$J(\omega_N) = \frac{1}{3d' + c'}\left[R_1 - \frac{7}{5}R_{noe}\right] \quad (14)$$

$$J(\omega_H) = \frac{1}{5d'}R_{noe} \quad (15)$$

where

$$R_{noe} = (\{^1H - ^{15}N\}NOE - 1)R_1 \cdot (\gamma_N/\gamma_H) \quad (16)$$

The constants c′ (= c^2) and d′ (= $d^2/4$) are approximately equal to 1.25 × 10^9 (rad/s)^2 and 1.35 × 10^9 (rad/s)^2, respectively, at 14.1 T.[29] Errors for the spectral density functions were calculated from the error in the relaxation parameters and by solving Eqs. 13–15, as given above.

RESULTS AND DISCUSSION

^{15}N R_1, R_2, and NOE of Barstar

A sample 2D HSQC spectrum of barstar at 305 K, pH 6.7 used to measure ^{15}N relaxation is shown in Figure 2. Excluding Pro 27, Pro 48, and the N-terminal residue from a total of 89 amino acids of barstar, 86 cross peaks should be resolved. Exchange broadening has been implicated in nonobservation of signals for certain residues, including Ile 86, Leu 88, and Ser 89.[7,11] Consistent with the previous report on the assignment of ^{15}N resonances in barstar we identify 75 ^{1}H-^{15}N backbone cross peaks, of which 69 nonoverlapping peaks were chosen for further analysis. Examples of decay of cross peak intensities as a function of inversion recovery delays in T_1 experiments and CPMG delays in T_2 experiments are shown in Figure 3 for three resonances, Ala 25, Cys 40, and Cys 82. The solid lines through the data are single-exponential fits according to Eq. 1.

The calculated R_1 and R_2 values and NOEs for all 69 ^{15}N sites are shown as bar graphs in Figure 4 and are also supplied as Supporting Information (Table I). As is observed commonly for native proteins, the R_1 values are fairly constant throughout the sequence and cannot be used directly to sense the motional properties of the protein chain. The R_2 values are also uniform except for residues Ile 13, Glu 28, Tyr 29, Gly 31, Asn 33, Arg 54, Glu 57, Thr 63, Asn 65, and Gly 66, which show larger values of R_2. Particularly striking are residues Tyr 29 and Thr 63, the R_2 values of which are twice the average of the remainder of the residues. Large values of R_2 most likely originate from chemical exchange when the exchange rate is faster than the CPMG repetition rate.

In the absence of conformational exchanging motions, and provided that the extreme narrowing condition for fast internal motions ($\omega_0\tau_i \ll 1$, where ω_0 is the Larmor frequency, and τ_i is the correlation time for the internal motion of the ith NH vector) is satisfied, the correlation frequencies for internal motions affect R_1 and R_2 to the same extent. Under these conditions the R_2:R_1 ratio depends only on the overall molecular tumbling correlation time, τ_m.[45,46] Thus, the R_2:R_1 ratio provides a useful initial estimate of τ_m. Residues with large-amplitude internal motions in a timescale longer than a few hundred picoseconds, which can be identified by low NOE values, must be excluded from this analysis. In addition, the residues for which R_2:R_1 ratio > 1.5 SD, where SD is standard deviation, also must be excluded from the above calculation, because these are likely to have conformational exchange contribution to the R_2 values. By following the above procedures, the mean R_2:R_1 ratios were found to be 3.7 ± 0.29. The ratio yielded the initial estimate of τ_m of 5.14 ± 0.28 ns for barstar, which was optimized later.[39] Figure 5 shows the R_2:R_1 ratio as a function of the amino acid sequence of barstar. Because R_1 values are fairly uniform across the sequence but R_2 values are not, the R_2:R_1 ratio is not expected to be uniform. Higher values are observed for residues Glu 28, Tyr 29, Gly 31, Asn 33, Tyr 47, Arg 54, Thr 63, Asn 65, Gly 66, and Thr 85.

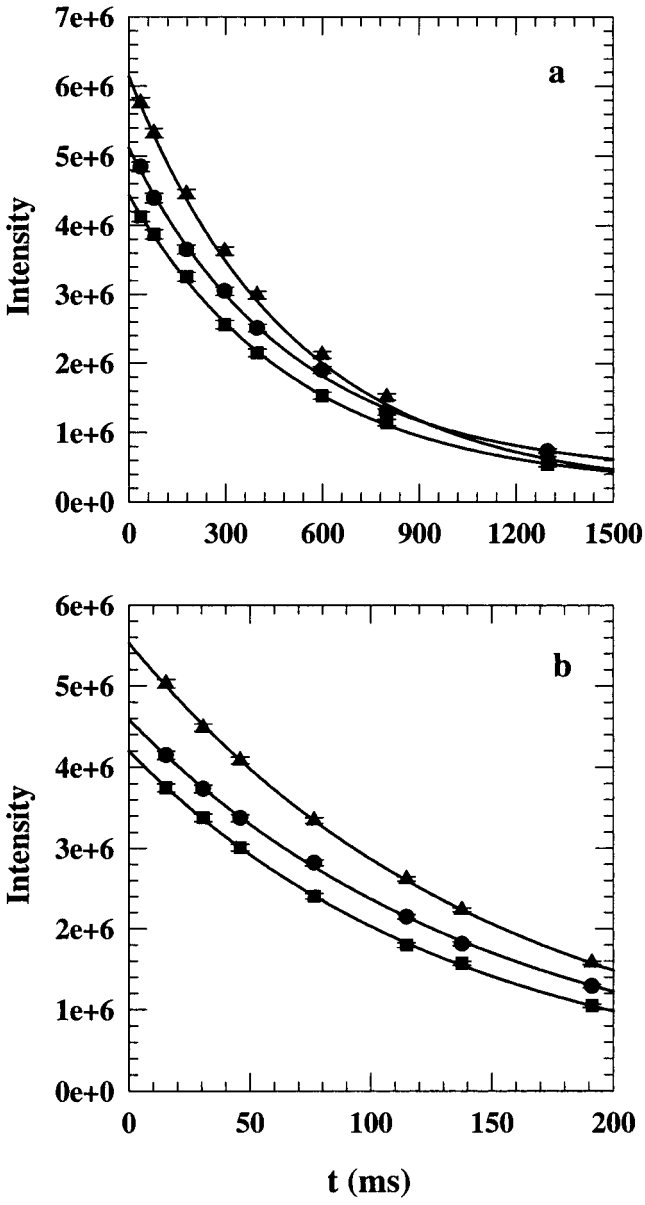

Fig. 3. ^{15}N relaxation data for the measurement of R_1 and R_2. **a:** T_1 relaxation data. **b:** T_2 relaxation data. Data for A25 (●), C40 (■) and C82 (▲) are shown. Intensities in arbitrary units are plotted against relaxation delays. The solid lines represent least-squares nonlinear exponential fits of the data to single exponential.

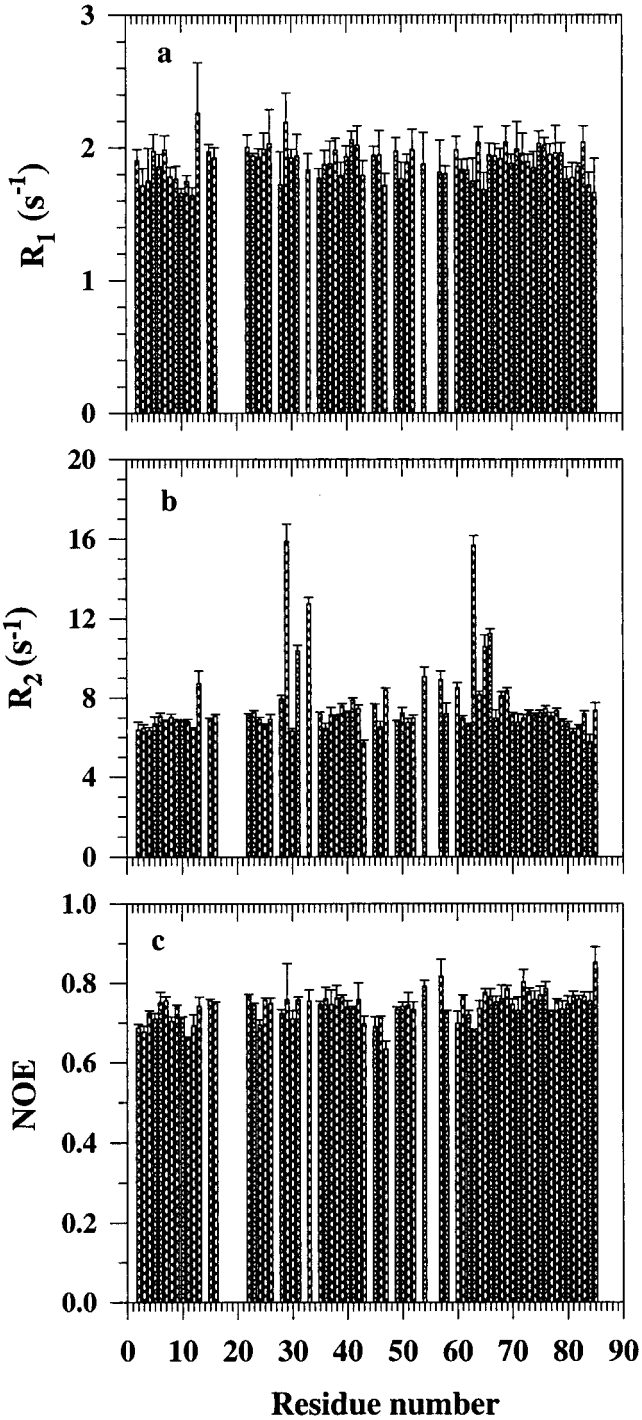

Fig. 4. Relaxation parameters for barstar. The values of (**a**) R_1, (**b**) R_2, and (**c**) proton-irradiated NOE for individual residues are shown as a function of residue number in the protein sequence. Errors in the measured relaxation parameters are also shown.

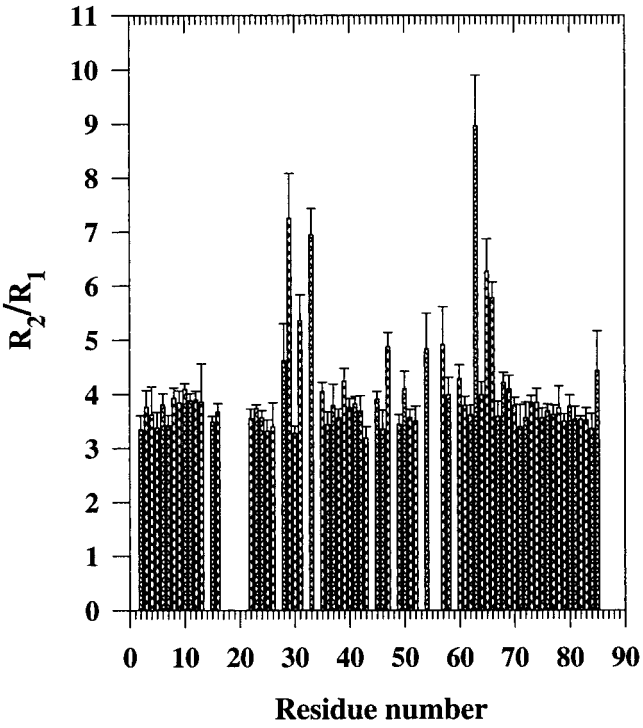

Fig. 5. R_2:R_1 ratio for individual residues as a function of residue number in the protein sequence of barstar.

Model-Free Analysis of R_1, R_2, and NOE

Isotropic versus axially symmetric models for rotational diffusion of barstar

Parameters defining the dynamics of the protein chain were extracted from extended model-free analysis of the primary relaxation data.[12–14] If the rotational diffusion is anisotropic and not included in the analysis, erroneous conclusions would be arrived at exchange rates. The errors introduced have been estimated by fitting simulated data, and it is observed that for a rigid nonspherical body, R_2 is underestimated by 20% for anisotropies with $D_\parallel/D_\perp$ equal to 2.0.[46] For moderate anisotropies, estimates of order parameters may be tolerant to the assumptions of isotropic motions, but the internal correlation time (τ_e) may be overestimated and the exchange contribution may be artificial, because both conformational exchange and anisotropic motion contribute to the measured R_2 values.

Barstar is an axially symmetric ellipsoid with the overall molecular dimension of $29 \times 22 \times 21$ Å.[7] The values for barstar are $D_{zz} = 1.0$, $D_{xx} = 0.75$, and $D_{yy} = 0.78$. The diffusion tensor constants parallel and perpendicular to the unique axis of the diffusion tensor are given by $D_\parallel = D_{zz} = 1.0$, and $D_\perp = 0.5(D_{xx} + D_{yy}) = 0.765$. The tensor is thus axially symmetric with diffusion anisotropy $D_\parallel/D_\perp \approx 1.3$. From the existing structural data of barstar (1bta.pdb), the initial estimates of the principal components of the inertial tensors, calculated by the program pdbinertia 1.0, are 1.0:0.91:0.68. These values vary significantly from a sphere. The asymmetry was verified further by using the program R2R1_1.1, which uses the approach of Tjandra et al.[37] to determine the diffusion tensors for spherical and axially symmetric motional modes from experimental ^{15}N spin relaxation data. The program indicates a statistically better fit for the relaxation data (R_2:R_1 ratios here) by using the axially symmetric model over the isotropic model (F-statistics = 3), with the values for τ_m, $D_\parallel/D_\perp$, θ and ϕ as

5.22 ± 0.31 ns, 0.81± 0.33, 1.53 ± 0.09° and 3.36 ± 0.1°, respectively. Furthermore, in both cases no statistically significant improvement in the fully anisotropic model over axially symmetric diffusion was observed.

However, we notice a discrepancy in the value of $D_{\parallel}/D_{\perp}$ calculated from structural data (1.3) on the one hand and from the ^{15}N relaxation data (0.81) on the other. In other words, barstar rotates in solution as an oblate ellipsoid of revolution and not as a prolate ellipsoid expected from the shape of the molecule. But the description of barstar as a prolate ellipsoid from structure itself is really an approximation. It just gives an idea of the degree of anisotropy. It is possible that the molecule does rotate as an oblate ellipsoid in solution. It also may appear that the observed discrepancy is caused by the inability of the axially symmetric model to distinguish between a prolate and an oblate ellipsoid because more than one minimum may be present in the conformational space.[47] But in our case, of the two minima observed during the fitting of R_2/R_1 data of only structurally well-defined residues, statistically better fit was observed for the one with oblate ellipsoidal rotation of barstar.

Starting from the above initial estimates of τ_m, $D_{\parallel}/D_{\perp}$, θ and ϕ, we analyzed the ^{15}N relaxation data by using both the isotropic and axially symmetric models for rotational diffusion tensor as described in Materials and Methods. The parameters were iteratively refined along with S^2 and τ_e parameters to fit the R_1, R_2, and NOE data according to model selection procedure described by Mandel et al.[39] This comparative study of isotropic versus axially symmetric models for rotational diffusion yielded the following results. (a) In going from the isotropic to the axially symmetric case, the average order parameters changed from 0.84 to 0.85 for barstar. (b) Conformational exchange was necessary for 12 residues in the isotropic case, whereas it was only for 7 residues in the axially symmetric case. (c) The results for the contribution of τ_e were merely similar in both the cases.

Keeping in mind the observation that the rotational diffusion tensor is not isotropic and the axially symmetric tensor yielded a better fit of the relaxation data, we discuss below the results obtained for the axially symmetric case only. The final optimized parameters τ_m and $D_{\parallel}/D_{\perp}$ for barstar was 5.2 ± 0.03 ns and 0.82 ± 0.03, respectively. But the optimized values of θ and ϕ, 82.7 ± 5.6 and 84.4 ± 7.1, respectively, show large deviation from the inputs of 1.53 ± 0.09° and 3.36 ± 0.1°, estimated from the experimental R_2/R_1 data by using the program R2R1_1.1. This observation indicates substantial reorientation of the axis during optimization by model-free analysis. We repeated the optimization exercise with the same inputs, estimated from R2R1_1.1, by using the program TENSOR developed by Marion and coworkers. TENSOR optimizes values of only three parameters, $D_{\parallel}/D_{\perp}$, θ, and ϕ, and the optimized values for two minima are: minimum 1: $D_{\parallel}/D_{\perp} = 0.87$, $\theta = 62.39 \pm 17.2$, $\phi = -66.56 \pm 17.07$; Minimum 2: $D_{\parallel}/D_{\perp} = 0.80$, $\theta = -14.93 \pm 18.38$, $\phi = 75.27 \pm 25.62$. These results do indicate that the molecule rotates as an oblate ellipsoid, but there is considerable uncertainty about the degree of orientation of the unique axis of the diffusion tensor. Better values of θ and ϕ could probably be obtained if the limitation of using a relatively smaller set of NH vectors for the estimation of the R_2:R_1 ratio did not exist.

Four different spectral density functional models were required to fit the experimental relaxation data. Model 1, in which S^2 is the sole fitting parameter, best describes the data for 20 NH vectors. Model 2, for which S^2 and τ_e are the parameters, best describes the relaxation of 42 NH vectors. Model 3 includes S^2 and R_{ex} and best describes the relaxation of 5 NH vectors. Model 4, which includes S^2, τ_e, and R_{ex}, was needed to fit the relaxation of only two NH vectors. The model-free parameters are plotted in Figure 6a, c, and d, and tables listing these values are supplied as Tables II and III Supporting Information. Some of these parameters are described below explicitly.

The internal correlation time parameter, τ_e

Although all residues experience some degree of fast internal motion, explicit inclusion of the internal correlation time parameter, τ_e, was needed to model the relaxation of 44 NH vectors, and the values are in the range 10.13 ± 6.02 ps to 143.74 ± 44.17 ps (Fig. 6c). In the absence of a well-defined model of motion τ_e is not readily interpretable, because it is related to both the rate and amplitude of internal motion faster than τ_m.

Overall rotational correlation time, τ_m

Each of the four function models used in the analysis contains τ_m, and its optimized value is 5.2 ± 0.03 ns. The isotropic value calculated for 20°C by the use of the equation, $\tau_m = V_h\eta/kT$, where V_h and η, respectively, are hydrated molecular volume (6×10^{-23} cc) and the solution viscosity (0.01 poise at 20°C)[48] is 4.3 ns. The deviation of the measured τ_m from the calculated one arises mainly because native barstar is not exactly globular at neutral pH. Persistence of some degree of diffusion anisotropy ($D_{\parallel}/D_{\perp} \approx 0.82$) has been discussed above. In previous time-resolved measurements of decay of fluorescence anisotropy of wild-type barstar at pH 7.0, 25°C, a τ_m value of 4.1 ns was reported.[49] The reason for the discrepancy in the values of τ_m determined by nitrogen spin relaxation and tryptophan fluorescence anisotropy is not clear. If the surrounding of the tryptophan indole(s) is significantly mobile, then it is possible that a lower value of τ_m will be obtained. Another possible reason for the higher value of τ_m found here could have been aggregation of barstar at the NMR concentration (1 mM, pH 6.7). We, however, did not observe any aggregation or precipitation of the protein during the course of data collection in this study and in our previous NMR experiments.[8,9] Also, dynamic light-scattering measurements of the protein solution under conditions used for NMR spectroscopy do not indicate protein aggregation.

The R_{ex} term

In general, ^1H-^{15}N dipolar and CSA relaxation mechanisms can account for transverse relaxation of the ^{15}N nuclei. The R_{ex} term is systematically added during data

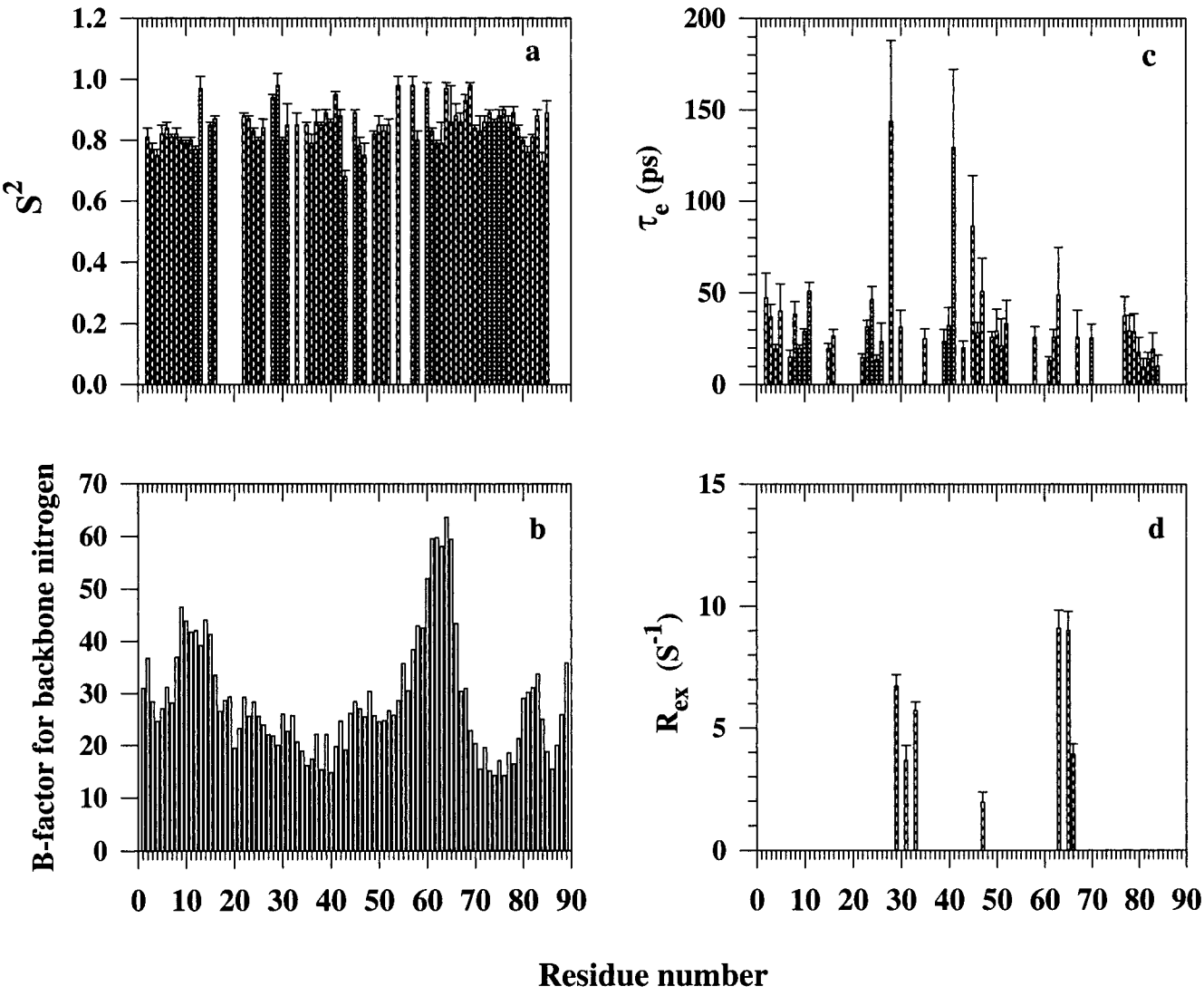

Fig. 6. Parameters defining the backbone dynamics of barstar. The order parameter, S^2 (**a**), the X-ray B-factors for backbone nitrogens (**b**), the internal correlation time τ (**c**), and the chemical exchange contribution, R_{ex} (**d**) for each amino acid residue is plotted as a function of residue number in the protein sequence.

analysis to improve the overall agreement between theory and experiment. Thus, the accuracy and significance of R_{ex} values are of concern. The model selection protocol that we have followed does not robustly identify values of $R_{ex} < 0.5$ s^{-1}.[50] The values for seven residues reported herein range from a minimum of 1.96 ± 0.41 s^{-1} to a maximum of 9.1 ± 0.75 s^{-1} (Fig. 6d) and can be interpreted confidently.

The distribution of S^2

Figure 6a displays sequence distribution of the S^2, the order parameter for angular motion, as a bar graph. The values range from 0.68 ± 0.02 for G43 to 0.98 ± 0.03 for R54 and E57. The surprisingly high-order parameter for R54 and E57 appear to indicate fully restricted motion of the two NH vectors, because both isotropic and axially symmetric models of rotational diffusion yielded similar values of S^2. But the possibility that such high values of S^2 could be a reflection of limitations of the model selection procedure in the model-free analysis is not precluded. The corresponding semiangles of rotation of these vectors in the "free diffusion in the cone" model,[12,13,51,52] calculated from the relation $S^2 = [0.5 \cos\theta\ (1+\cos\theta)]^2$, range from $\approx 28.6°$ to 6.6°. The average values of S^2 for different secondary structural elements in the protein, and of the set of barnase-binding residues and the set of completely buried residues that comprise the hydrophobic core of the protein are listed in Table II. In general, the order parameter is fairly independent of secondary structures. The average value of S^2 is smallest for β-strand 1 (0.80 ± 0.03) and smaller for β-strand 3 (0.83 ± 0.09). The overall average value of 0.85 (± 0.02) is close to those reported for several other proteins, including Snase,[53] eglin c,[16] *C.*

TABLE II. Order Parameters for Secondary Structural Elements, the Barnase-Binding Residues, and the Hydrophobic Core

Structure	Sequence	No. of residues averaged	S^2
β-strand 1	1–7	6	0.80 (±0.03)
α-helix 1	12–25	7	0.86 (±0.02)
α-helix 2	33–44	10	0.85 (±0.06)
β-strand 2	49–54	5	0.86 (±0.07)
α-helix 3	55–63	6	0.86 (±0.08)
α-helix 4	66–81	16	0.86 (±0.05)
β-strand 3	83–89	3	0.83 (±0.09)
Barnase-binding residues	29–46,73,76	17	0.86 (±0.07)
Hydrophobic core residues	3,5,10,16,20,24,26,34,37,41,45,49, 51,53,56,67,70,71,73,74,77,84,86	18	0.84 (±0.05)

maxima trypsin inhibitor,[54] and chymotrysin inhibitor 2.[55]

Comparison of S^2 Values With Crystallographic B-Factors

The X-ray B-factors for the backbone nitrogens of wild-type barstar, kindly made available by Dr. Y. Mauguen and colleagues, are shown in Figure 6b. Several backbone dynamics studies have searched for the inverse correlation between NH order parameters and B-factors for backbone atoms of the same protein. The degree of correlation varies to a large extent. For example, in *E. coli* RNase H the qualitative correlation between order parameters and B-factors is moderately high.[39] S^2 values correlate inversely with crystallographic B-factors in the case of calbindin D*9k* also.[56] On the other hand, little or no correlation has been identified for *E. coli* thioredoxin,[57] and oxidized flavodoxin from *A. nidulans*.[40] In the present study also, we identify no apparent correlation, except that a minor inverse correlation is noticeable along β-strand 1 (Table II and Fig. 6a and b). Despite the existence of little correlation between crystal B-factors and S^2 values, the former are comparable with the NMR B-factors $(= \frac{8\pi^2}{3})\langle \text{rmsd} \rangle^2$ for the backbone heavy atoms. The regions of the large values of NMR for the backbone[7,11] coincide with the major peaks in the crystal B-factor profile. However, the dynamics of the barnase-binding residues (residues 29–46, 73, and 76) are not particularly delineated by B-factors of NMR or X-ray crystal structures. The large X-ray B-factors for the backbone nitrogens of the loop connecting helices 3 and 4 (residues 64–67) correlate most strikingly with the observation of large root mean square deviation of the backbone atoms from the mean atomic NMR structure. This ill-defined loop is the worst defined region of the structure of barstar.[7]

As has been suggested,[39,40] the varying degrees of inverse correlation between S^2 and B-factors arise mainly from the insensitivity of order parameters to translational displacements. In fact, because the frequency of Larmor precession of nuclei match only the frequencies of rotational motions, the faster processes including bond vibrations do not affect the order parameter. NMR relaxation is also limited to the detection of motions that are faster than the overall correlation time. On the other hand, the B-factor is primarily a consequence of effects other than internal protein motions. The sources of the B-factor are (a) crystal mosaicity, (b) dynamic disorder in the crystal produced by the temperature-dependent vibrations of atoms, and (c) static disorder produced by nonequivalent occupancy of protein molecules, or parts of molecules, in different unit cells. The effect of static disorder on the X-ray diffraction pattern is not distinguishable from the effect of dynamic disorder unless intensity data at different temperatures are collected.[58]

Conformational Entropy of Wild-Type Barstar

Yang and Kay[59] described relations between NMR-derived order parameters and conformational entropy for several models of bond vector motions. For the conformational entropy, S_{conf}, arising from ps timescale motion of the NH bond vectors, assuming the bond motion to be confined to a cone, the following equation has been derived.[59]

$$S_{\text{conf}} = R \ln[\pi\{3 - (1 + 8S)^{0.5}\}] \quad (17)$$

where R is the gas constant and S is the square root of the order parameter. This formula assumes that the motions of the individual NH vectors are independent, which may lead to an overestimate of the entropy value. Furthermore, the above equation is valid when the value of $S^2 < 0.95$. Conformational entropies (may also be called librational entropy) of 61 residues of barstar, for which $S^2 < 0.95$, are shown in Figure 9c. The values range from -17.5 to -2.3 cal mol^{-1} K^{-1}. In general, an increase in the order parameter results in loss of entropy and vice versa. Although this provides a simple picture of NH vector motional contribution to entropy, and thus to free energy, this number cannot be taken to imply an overall entropic contribution, because (a) all the vectors in the molecule are not considered because S^2 values are not available for all residues, (b) the equation is applicable only for $S^2 < 0.95$, (c) the motions of individual vectors are not necessarily independent, (d) the order parameters do not reflect motions outside the ns-ps timescale, and (e) solvent ordering (disordering) is not included.

The entropic contribution of subnanosecond timescale motions to the stability of a protein is the difference between two absolute entropies. Here, we have values of S_{conf} only for 61 residues of native barstar, which contribute 160 kcal mol^{-1} at 305 K to the residual entropy of the protein. This indicates that the local residual entropy of a protein can be large and arise from states interconverting on fast timescale.

Reduced Spectral Density Mapping

The bar graphs in Figure 7 show the three spectral densities as a function of amino acid sequence of barstar. The interpretation of these results in molecular motions is based on the shape of the spectral density curve, and the distribution of relaxation parameters is a function of frequencies of molecular motions. In a protein, the area under the spectral density curve, a Lorentzian function of frequency, is a constant and does not vary from one NH vector to another.[40,60] Therefore, for a given NH vector, the spectral density at the Larmor frequency ω will decrease as the NH reorientation rate becomes substantially faster or slower than ω. Thus, R_1, R_2, and $\{^1H\}$-^{15}N NOE are dominated, respectively, by $J(\omega_N)$, $J(0)$, and $J(\omega_H)$. The constant value of the area under the $J(\omega)$ curve also requires that smaller values of $J(0)$ are compensated by larger values of spectral densities at higher frequencies,[40] suggesting that the residues having smaller $J(0)$ values indicate faster internal motions at frequencies approaching ω_N and ω_H. As seen in Eq. 13, $J(0)$ includes the contributions from chemical exchange and other pseudo first-order processes (R_{ex}) to R_2, which is not considered explicitly in the calculations. Thus, an increase in $J(0)$ can be caused by a relatively slower rotational fluctuation of NH vector on an ns timescale and/or pseudo first-order processes that occur on a micro- to millisecond timescale. Residues Ile 13, Glu28, Tyr 29, Gly 31, Asn 33, Tyr 47, Arg 54, Glu 57, Lys 60, Thr 63, Glu 64, Asn 65, Gly 66, Glu 68, and Ser 69 have distinctly higher values of $J(0)$, indicating that chemical exchange motions have significant contributions to the mobility of their NH vectors. This result is consistent with the primary relaxation data (Fig. 4b) that all these residues have larger values of R_2.

Determination of τ_m from the reduced spectral density map

A linear correlation between $J(\omega_{N,H})$ and corresponding $J(0)$ values has been proposed by Lefèvre et al.[18] Figure 8 shows these correlations for barstar. The solid lines are linear least squares fit of the data according to $J(\omega_{N,H}) = \alpha J(0) + \beta$. The apparent scatter in the data arises from the expansion of axes scales. The crowding of the data within a narrow region in both plots simply indicates less inhomogeneity in NH mobility throughout the backbone, because the magnitude of reduced spectral densities are affected only by the values of the primary relaxation parameters (Eqs. 13–15). The α- and β- values from the plot of $J(\omega_N)$ versus $J(0)$ were found to be 0.0772 and 0.2182 ns/rad, respectively, and were used to calculate τ_m, the overall molecular tumbling correlation time, from the equation:[18,40]

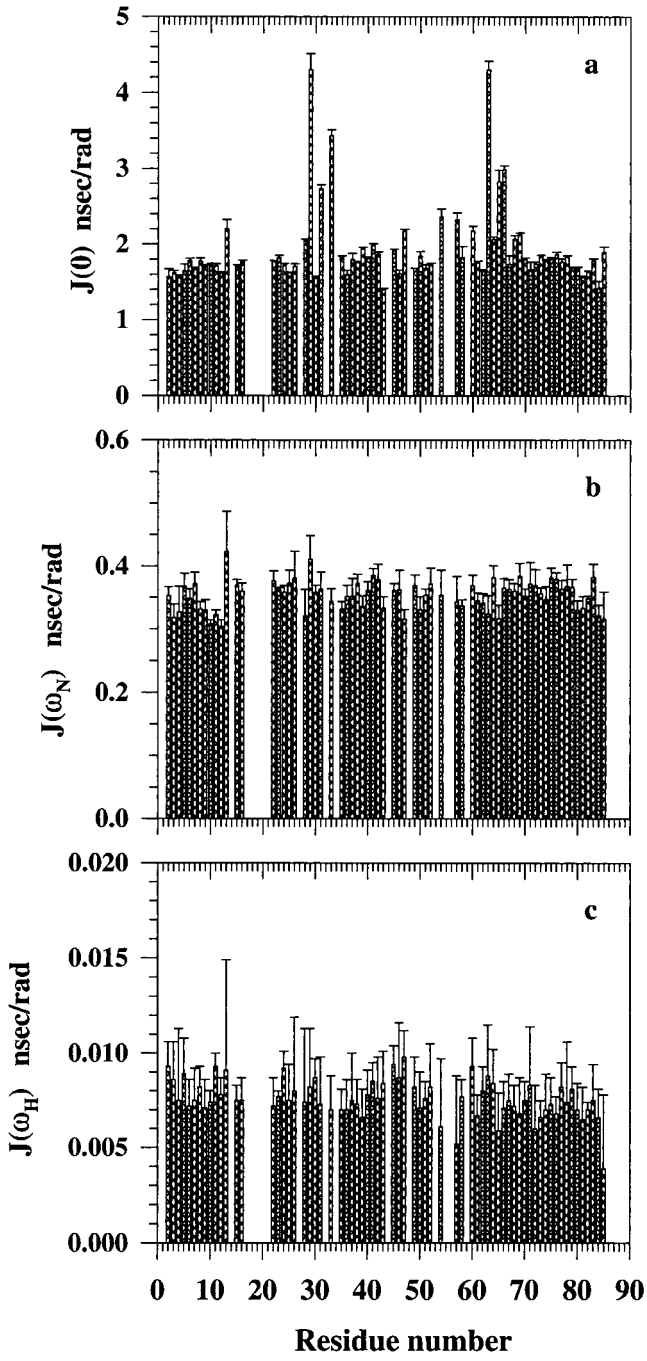

Fig. 7. **a–c:** Bar graphs of the spectral density functions from the reduced spectral density mapping as a function of sequence number. Y-axes of these plots have different scales.

$$2\alpha\omega_N^2\tau_m^3 + 5\beta\omega_N^2\tau_m^2 + 2(\alpha - 1)\tau_m + 5\beta = 0 \qquad (18)$$

The correlation coefficient of the above regression analysis was only 21.8 %. The solution of the above cubic equation, yielded three values of τ_m: −14.4, 0.6, and 5.7 ns, out of which the most realistic value of 5.7 ns was chosen for τ_m.

The value of τ_m = 5.7 ns is greater than that determined from the model-free analysis by 0.5 ns. This value is only

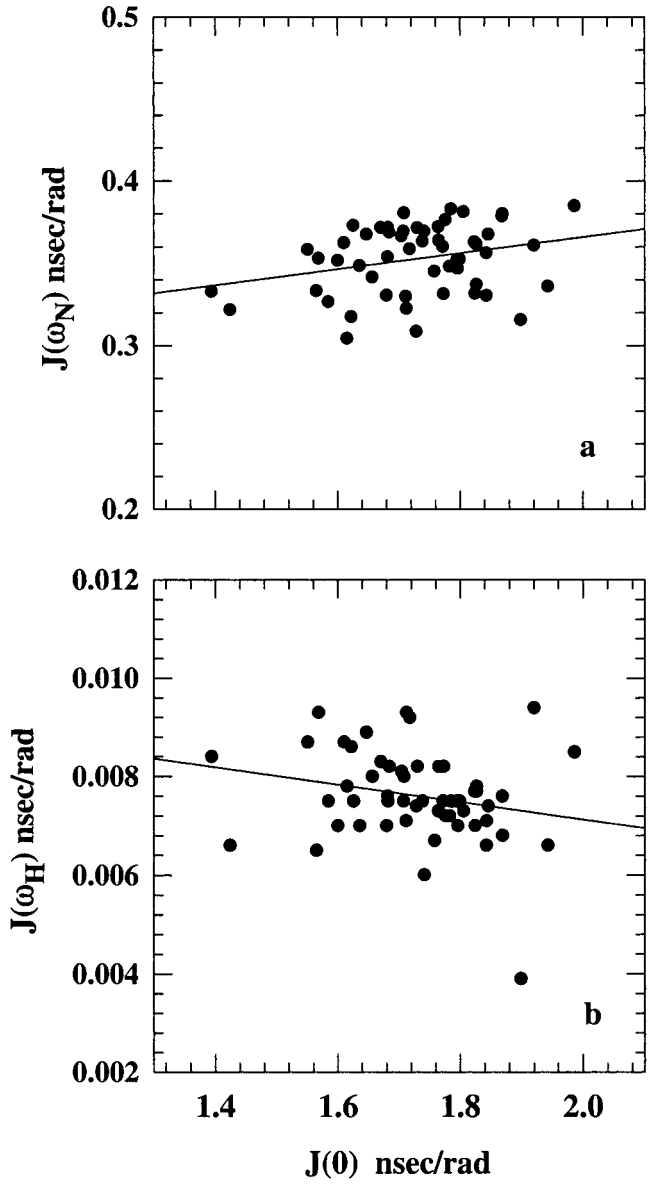

Fig. 8. Plots of (**a**) $J(\omega_N)$ versus J(0) with $\alpha = 7.72e\text{-}2$, $\beta = 0.2182$; and (**b**) $J(\omega_H)$ versus J(0) with $\alpha = -1.656e\text{-}3$, $\beta = 1.046e\text{-}2$. The correlation coefficient for the fit is 21.8%. The residues with large J(0) values are not included in the plots. The fit was obtained by linear regression. Here α is slope and β is intercept along ω_N or ω_H axis.

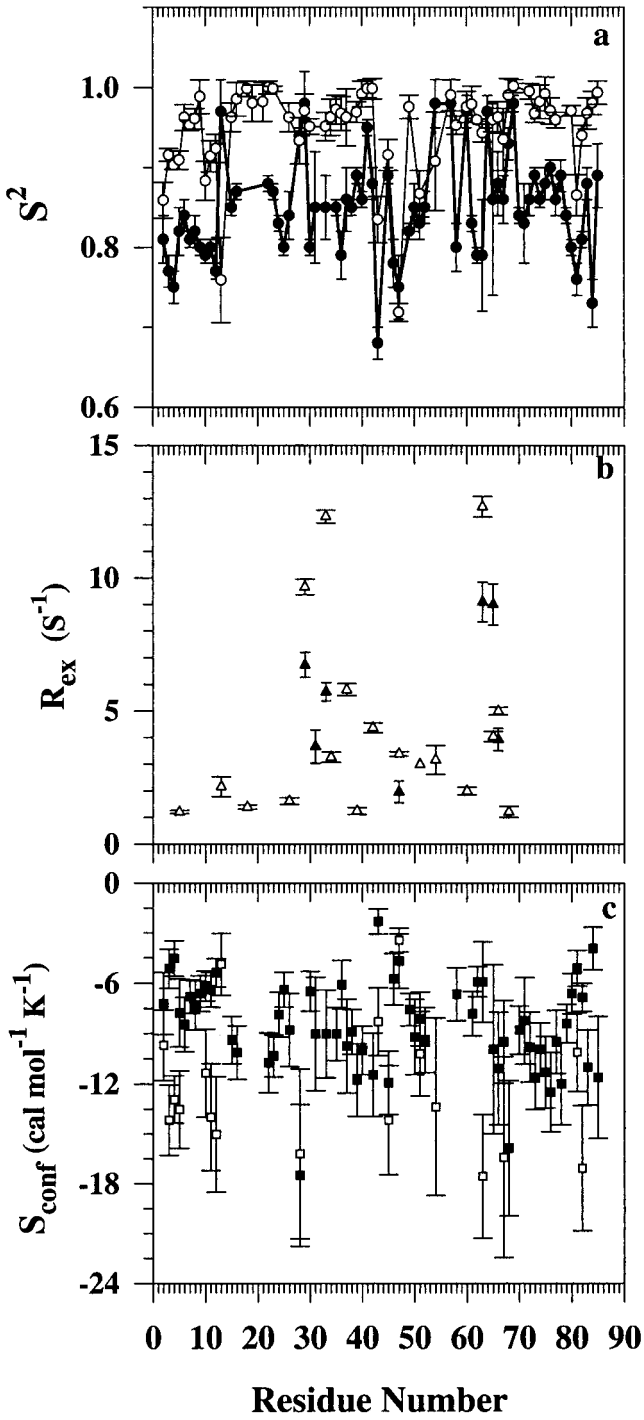

Fig. 9. A comparison of the values of S^2 (**a**), R_{ex} (**b**), and S_{conf} (**c**) for the wild-type (closed symbols) and the C40/82A mutant (open symbols) of barstar.

≈10% higher than those obtained by model-free analysis. Similar increase has been found in the case of a backbone dynamics study of barnase (unpublished result). The difference could be in part due to the lack of good correlation as seen from Figure 8. Nonetheless, the reasonable concurrence between the two estimates provides certain degree of validation of assumptions involved in both the approaches.[40]

Comparison of Backbone Dynamics of Wild-Type Barstar and C40/82A Mutant

We compare the present results on wild-type barstar (1 mM, 20 mM phosphate, pH 6.7, 32°C) obtained at a magnetic field strength of 14.10 T with the results of Wong et al.[11] who used ^{15}N relaxation data at 11.74 T and 14.10 T to determine the dynamics of the C40/82A mutant of barstar (2.0–3.5 mM, 10 mM phosphate, pH 6.7, 30°C). The values of S^2 for wild-type and C40/82A mutant proteins, plotted in Figure 9a, are generally higher for

most residues of the mutant protein, several of which appear to approach a value of 1.0. The mean values of S^2, averaged over 69 NH vectors of the wild-type and 61 NH vectors of the mutant protein, are 0.85($\pm$0.06) and 0.95($\pm$0.05), respectively. The errors indicate that the mean values of S^2 from the two studies may tend to approach each other. Differences in values of S^2 of individual NH vectors may originate from uncertainties in the overall correlation time (5.2 ns for the wild-type and 5.5 ns for the mutant protein,[11] both determined from extended model-free analysis) or the neglect of the anisotropic diffusion in the case of the mutant. The plots in Figure 9a show that differences in the patterns of the relative S^2 values exist, clearly noticeable for residues 40–85, which appear to suggest the existence of motional differences between the two. However, all residues in both wild-type and mutant proteins experience some degree of fast internal motion. Even those residues that yield $S^2 = 1$ (Fig. 9a) are likely to experience fast internal motion, because a S^2 value of 1.0 is unrealistically high and likely to be a fitting artifact. We must mention that this comparison, based on the data made available by Wong et al.,[11] may not be straightforward, given that the protein concentration for NMR spectroscopy used by these authors is at least twofold higher than used in this study. If there was any aggregation of the mutant protein, the simple comparison presented here will not be useful.

The transverse relaxation rates at 14.10 T for all residues in the mutant are larger than those for the wild-type protein. The R_2 rates range from 7.2 to 26 s^{-1} in the mutant and from 5.71$\pm$ 0.13 to 15.88 $\pm$ 0.86 s^{-1} in the wild-type protein. Large R_2 values for residues Tyr 29, Asn 33, Arg 54, Thr 63, Asn 65, and Gly 66 were observed in both of these studies. Thus, both studies provide evidence for substantial chemical exchange motions in the barnase-binding loop (residues 29–33) and in the loop connecting the third and fourth helix (Thr 63, Asn 65, and Gly 66). The general trend of relatively larger R_2 rates, if not due to a systematic error, reported for all residues of C40/82A suggests, however, the presence of conformational exchanging motions throughout the backbone of the mutant. In the model-free analysis of the relaxation data for the mutant protein the R_{ex} term was used for 59 residues; the values ranging from less than 1 s^{-1} for most NH vectors to $\approx$13 s^{-1}. Because of the neglect of anisotropy in the analysis and errors associated with the determination of relaxation rates, and therefore with the overall correlation time, the exchange contribution of $<$1.0 s^{-1} in the study of Wong et al.[11] may be considered insignificant. In Figure 9b the R_{ex} values $>$1 s^{-1} are compared for the mutant and the wild-type protein. R_{ex} values for the residues in the mutant protein are somewhat larger. Also, additional residues in the mutant protein display exchanging motion. The values of τ_m obtained from model-free analysis are 5.5 and 5.2 ns for the mutant and the wild-type protein, respectively. Reduced spectral density analysis of the wild-type relaxation data in the present study yielded a τ_m value of 5.7 ns.

To facilitate a residuewise comparison of conformational entropy of the wild-type and the C40/82A mutant, we calculated S_{conf} values for the C40/82A mutant by using the relaxation data published by Wong et al.[11] Figure 9c presents the comparison. In the case of wild-type barstar, of 69 NH vectors for which the value of S^2 has been calculated, 61 vectors have $S^2 < 0.95$, whereas for the C40/82A mutant, S^2 is available for 61 residues, and for most of them (43 residues) $S^2 \geq 0.95$. Thus, in Figure 9c only 18 NH vectors figure for the comparison of S_{conf}. Of these 18, only 9 residues show significant difference in librational entropy. It is possible to estimate the entropic contribution of subnanosecond motion of NH vectors to the stability difference between the wild-type and the mutant barstar, but the availability of the S_{conf} value for only a fewer residues precludes obtaining a useful estimate.

We point out that the relaxation data were collected at 30°C for the mutant[11] and at 32°C for the wild-type protein; the offset of 2°C existed because we had completed data collection at the time the results of the mutant protein[11] were published. The temperature offset may appear to contribute to the differences in the R_2 rates observed for the two proteins, but the temperature difference is small and will make a minor contribution only.

These observations are interesting because solution NMR structures of the wild-type and the C40/82A mutant protein are superimposable.[7,10] The two proteins are similar in terms of stability: ΔG^{H2O}, the free energy of unfolding in water as determined by urea denaturation experiments, is 4.84 $\pm$ 0.18 kcal mol^{-1} for the mutant,[3] and 4.7 $\pm$ 0.25 kcal mol^{-1} for the wild-type protein (unpublished data). The mutant exhibits normal barnase inhibitory activity. In the wild-type protein the two cysteines, C40 and C82, are relatively buried with solvent accesibilities of 5% and 25%, respectively, and mutations in these regions of the protein appear to affect local dynamics throughout, even though according to Wong et al.[11] the Cys-to-Ala replacement does not produce any significant structural change. Similar observations in the case of thioredoxin have been reported by Lorimier et al.[61] These authors observe that the structures of wild-type thioredoxin and its L78K mutant are largely similar, even though the mispacking of the protein core in one location affects local dynamics and stability throughout the backbone of the protein. These observations raise the question: how does a slight packing perturbation affect local NH rotational dynamics at sites distant along the backbone?

Function and Backbone Dynamics of Barstar

Putting the backbone motional parameters in the perspective of the known biological functions of proteins is an essential aspect of relaxation dynamics studies. The dynamic properties observed in this study do not appear to be consistent with dynamics expected of the amino acids forming the barnase-binding region (residues 29–46, 73, and 76), given that barnase-barstar binding is extremely tight.[2,3] Protein-protein and protein-ligand complexation typically leads to a decrease in segmental flexibility; accordingly, one may expect larger values of S^2 for the

barnase-binding residues. The results, though, do not show larger values for these residues (Figs. 6a and 9a). However, as indicated by high R_2 values and the requirement of the R_{ex} term to model the relaxation data, only three of the barnase-binding residues, Tyr 29, Gly 31, and Asn 33, display millisecond-microsecond segmental motions. This finding suggests the absence of widespread exchanging motions for the barnase-binding surface. Furthermore, the X-ray B-factors for the backbone nitrogens of barnase-binding residues have relatively smaller values. Thus, it appears that the barnase-binding surface on barstar is largely rigid. As discussed elsewhere,[62] binding site flexibility allows for broadened specificity. This may come at the price of reduced affinity due to the loss of conformational entropy on binding. Conversely, a rigid binding site should result in narrow specificity and tight binding for well-matched surfaces. The observation of certain degree of rigidity of the barnase-binding residues may contribute to the extremely tight binding between barnase and barstar ($K_d \approx 2 \times 10^{-14}$ M). It should also be realized that the dynamic properties related to the protein function cannot be described entirely on the basis of backbone dynamics alone. A complete analysis of the connection between dynamics and function will have to wait for a study of the side-chain dynamics of the protein. We have just concluded a ^{15}N NMR relaxation study of the dynamics of the barstar-barnase complex, the results of which will shed considerable light to the dynamic properties of the binding interface.

ACKNOWLEDGMENTS

The NMR spectra were recorded in the National Facility for High Resolution NMR, TIFR, Mumbai, supported by the Department of Science and Technology, Government of India. We thank Dr. R. V. Hosur for support, suggestions, and many useful discussions.

REFERENCES

1. Hartley RW. Barnase and barstar: two small proteins to fold and fit together. Trends Biochem Sci 1989;14:450–454.
2. Hartley RW, Smeaton JR. On the reaction betweeen the extracellular ribonuclease of *Bacillus amyloliquefaciens* (barnase) and its intracellular inhibitor. J Biol Chem 1973;248:5624–5626.
3. Schreiber G, Fersht AR. The refolding of *cis*-petidylprolyl and *trans*-peptidylprolyl isomers of barstar. Biochemistry 1993:32: 11195–11203.
4. Guillet V, Lapthorn A, Hartley RW, Mauguen Y. Recognition between a bacterial ribonuclease, barnase, and its natural inhibitor, barstar. Structure 1993;1:165–177.
5. Jones DNM, Bycroft M, Lubienski MJ, Fersht AR. Identification of the barstar binding site of barnase by NMR spectroscopy and hydrogen-deuterium exchange. FEBS Lett 1993;331:165–172.
6. Mariani C, Gossele V, Bebeuckeleer M, Deblock M, Goldberg RB. A chimaeric ribonuclease inhibitor gene restores fertility to male sterile plants. Nature 1992;357:384–387.
7. Lubienski MJ, Bycroft M, Freund SMV, Fersht AR. Three dimensional solution structure and ^{13}C assignments of barstar using nuclear magnetic resonance spectroscopy. Biochemistry 1994;33: 8866–8877.
8. Bhuyan AK, Udgaonkar JB. Two structural subdomains of barstar detected by rapid mixing NMR measurement of amide hydrogen exchange. Proteins: Struct Funct Genet 1998;30:295–308.
9. Bhuyan AK, Udgaonkar JB. Observation of multi-state kinetics during the slow folding and unfolding of barstar. Biochemistry 1999;38:9158–9168.
10. Lubienski MJ, Bycroft M, Jones DNM, Fersht AR. Assignment of the backbone ^{1}H and ^{15}N NMR resonances and secondary structure characterization of barstar. FEBS Lett 1993;332:81–87.
11. Wong K-B, Fersht AR, Freund SMV. NMR ^{15}N relaxation and structural studies reveal slow conformational exchange in barstar. J Mol Biol 1997;268:494–511.
12. Lipari G, Szabo A. Model-free approach to the interpretation of nuclear magnetic resonance relaxation in macromolecules. 1. Theory and range of validity. J Am Chem Soc 1982a;104:4546–4559.
13. Lipari G, Szabo A. Model-free approach to the interpretation of nuclear magnetic resonance relaxation in macromolecules. 2. Analysis of experimental results. J Am Chem Soc 1982b;104:4559–4570.
14. Clore GM, Szabo A, Bax A, Kay LE, Driscoll PC, Gronenborn AM. Deviations from the simple two-parameter model-free approach to the interpretation of nitrogen-15 nuclear magnetic relaxation of proteins. J Am Chem Soc 1990a;112:4989–4991.
15. Peng JW, Wagner G. Mapping of spectral density functions using heteronuclear NMR relaxation measurements. J Magn Reson 1992a;98:308–332.
16. Peng JW, Wagner G. Mapping of the spectral densities of N-H bond motions in eglin c using heteronuclear relaxation measurements. Biochemistry 1992b;31:8571–8586.
17. Farrow NA, Zhang O, Forman-Kay JD, Kay LE. Comparison of the backbone dynamics of a folded and an unfolded SH3 domain existing in equilibrium in aqueous buffer. Biochemistry 1995;34: 868–878.
18. Lefèvre J-F, Dayie KT, Peng JW, Wagner G. Internal mobility in the partially folded DNA binding and dimerization domains of GAL4: NMR analysis of the N-H spectral density functions. Biochemistry 1996;35:2674–2686.
19. Khurana R, Udgaonkar JB. Equilibrium unfolding studies of barstar: evidence for an alternative conformation which resembles a molten globule. Biochemistry 1994;33:106–115.
20. Vold RL, Waugh JS, Klein MP, Phelps DE. Measurement of spin relaxation in complex systems. J Chem Phys 1968;48:3831–3832.
21. Meiboom S, Gill D. Modified spin-echo method for measuring nuclear spin relaxation times. Rev Sci Instrum 1958;29:688–691.
22. Noggle JH, Schirmer RE. The nuclear Overhauser effect: chemical applications. New York: Academic Press; 1971.
23. Farrow NA, Muhandiram R, Singer AU, et al. Backbone dynamics of a free and a phosphopeptide-complexed Src homology 2 domain studied by ^{15}N NMR relaxation. Biochemistry 1994;33:5984–6003.
24. Cavanagh J, Palmer AG, Wright PE, Rance M. Sensitivity improvement in proton detected two-dimensional heteronuclear relay spectroscopy. J Magn Reson 1991;91:429–436.
25. Palmer AG III, Cavanagh J, Wright PE, Rance M. Sensitivity improvement in proton-detected two-dimensional heteronuclear correlation NMR spectroscopy. J Magn Reson 1991;3:151–170.
26. Marion D, Ikura M, Tschudin R, Bax A. Rapid recording of 2D NMR spectra without phase cycling: application to the study of hydrogen exchange in proteins. J Magn Reson 1989;85:393–399.
27. Palmer AG, Skelton NJ, Chazin WJ, Wright PE, Rance M. Suppression of the effects of cross-correlation between dipolar and anisotropy chemical shift relaxation mechanisms in the measurement of spin-spin relaxation rates. Mol Phys 1992;75:699–711.
28. Kay LE, Ikura M, Tschudin R, Bax A. Three-dimensional triple-resonance NMR spectroscopy of isotopically enriched proteins. J Magn Reson 1990;89:496–514.
29. Peng JW, Wagner G. Investigation of protein motions via relaxation measurements. Methods Enzymol 1994;239:563–596.
30. Markley JL, Horsley WJ, Klein MP. Spin-lattice relaxation measurements in slowly relaxing complex spectra. J Chem Phys 1971;55:3604–3605.
31. Skelton NJ, Palmer AG, Akke M, Kördel J, Rance M, Chazin WJ. Practical aspects of two-dimensional proton-detected ^{15}N spin relaxation measurements. J Magn Reson 1993;B102, 253–264.
32. Abragam A. Principles of nuclear magnetism. Oxford: Clarendon Press; 1961.
33. Hiyama Y, Niu C-H, Silverton JV, Bavoso A, Torchia DA. Determination ^{15}N chemical shift tensor via ^{15}N-^{2}H dipolar coupling in Boc-glycylglycyl[^{15}N]glycine benzyl ester. J Am Chem Soc 1988; 110:2378–2383.
34. Bloom M, Reeves LW, Wells EJ. Spin echoes and chemical exchange. J Chem Phys 1965;42:1615–1624.

35. Clore GM, Driscoll PC, Wingfield PT, Gronenborn AM. Analysis of the backbone dynamics of interleukin-1β using two-dimensional inverse detected heteronuclear ^{15}N-H NMR spectroscopy. Biochemistry 1990b;29:7387–7401.
36. Schurr JM, Babcock HP, Fujimoto BS. A test of model-free formulas: effects of anisotropic rotational diffusion and dimerization. J Magn Reson 1994;B105: 211–224.
37. Tjandra N, Feller SE, Pastor RW, Bax A. Rotational diffusiona anisotropy of human ubiquitin from ^{15}N NMR relaxation. J Am Chem Soc 1995;117:12562–12566.
38. Zheng Z, Czaplicki J, Jardetzky O. Backbone dynamics of *trp* repressor studied by ^{15}N NMR relaxation. Biochemistry 1995;34: 5212–5223.
39. Mandel AM, Akke M, Palmer AG III. Backbone dynamics of *Escherichia coli* ribonuclease H1: correlations with structure and function in an active enzyme. J Mol Biol 1995;246:144–163.
40. Zhang P, Dayie KT, Wagner G. Unusual lack of internal mobility and fast overall tumbling in oxidized flavodoxin from *Anacystis nidulans*. J Mol Biol 1997;272:443–455.
41. Peng JW, Wagner G. Frequency spectrum of NH bonds in eglin c from spectral density mapping at multiple fields. Biochemistry 1995;34:16733–16752.
42. Ishima R, Nagayama K. Protein backbone dynamics revealed by quasi spectral density function analysis of amide N-15 nuclei. Biochemistry 1995a;34:3162–3171.
43. Ishima R, Nagayama K. Quasi-spectral-density function analysis for nitrogen-15 nuclei in proteins. J Magn Reson Sect B 1995b;108: 73–76.
44. Farrow NA, Zhang OW, Szabo A, Torchia DA, Kay LEJ. Spectral density function mapping using ^{15}N relaxation data exclusively. Biomol NMR 1995;6:153–162.
45. Kay LE, Torchia DA, Bax A. Backbone dynamics of proteins as studied by ^{15}N inverse detected heteronuclear NMR spectroscopy: application to staphylococcal nuclease. Biochemistry 1989;28:8972–8979.
46. Tjandra N, Garrett DS, Gronenborn AM, Bax A, Clore GM. Defining long range order in NMR structure determination by diffusion induced relaxation anisotropy. Nat Struct Biol 1997;4: 443–449.
47. Blackledge M, Cordier F, Dosset P, Marion D. Precision and uncertainty in the characterization of anisotropic rotational diffusion by ^{15}N relaxation. J Am Chem Soc 1998;120:4538–4539.
48. Cantor RC, Schimmel PR. Biophysical chemistry. Vol. II. San Francisco: W. H. Freeman; 1980.
49. Swaminathan R, Periasamy N, Udgaonkar JB, Krishnamoorthy G. Molten globule-like conformations of barstar: a study of fluorescence dynamics. J Phys Chem 1994;98:9270–9278.
50. Mandel AM, Akke M, Palmer AG III. Dynamics of ribonuclease H: temperature dependence of motion on multiple time scale. Biochemistry 1996;35:16009–16023. 51. Kinoshita K, Kawato W Jr, Ikegami A. Theory of fluorescence, polarizatio decay in membranes. Biophys J 1977;20:289–305.
52. Dayie KT, Wagner G, Lefèvre J-F. Theory and practice of nuclear spin relaxation in proteins. Annu Rev Phys Chem 1996;47:243–282.
53. Kay LE, Muhandiram DR, Farrow NA, Aubin Y, Forman-Kay JD. Correlation between dynamics and high affinity binding in an SH2 domain interaction. Biochemistry 1996;35:361–368.
54. Liu J, Prakash O, Cai M, et al. Solution structure and backbone dynamics of recombinant *Cucurbita maxima* trypsin inhibitor-V determined by NMR spectroscopy. Biochemistry 1996;35:1516–1524.
55. Shaw GL, Davies B, Keeler J, Fersht AR. Backbone dynamics of chymotrypsin inhibitor 2: effects of breaking the active site bond and its implications for the mechanism of inhibition of serine proteases. Biochemistry 1995;34:2225–2233.
56. Kördel J, Skelton NJ, Akke M, Palmer AG III, Chazin WJ. Backbone dynamics of calcium-loaded calbindin D_{9k} studied by two-dimensional proton-detected ^{15}N NMR spectroscopy. Biochemistry 1992;31:4856–4866.
57. Stone MJ, Chandrasekhar K, Holmgren A, Wright PE, Dyson HJ. Comparison of backbone and tryptophan side-chain dynamics of reduced and oxidized *Escherichia coli* thioredoxin using ^{15}N NMR relaxation measurements. Biochemistry 1992;31:4394–4406.
58. Drenth J. Principles of protein x-ray crystallography. New York: Springer-Verlag; 1994.
59. Yang D, Kay LE. Contributions to conformational entropy arising from bond vector fluctuations measured from NMR-derived order parameters: application to protein folding. J Mol Biol 1996;263: 369–382.
60. Slichter CP. Principles of magnetic resonance. New York: Springer Verlag; 1990.
61. Lorimier RD, Hellinga HW, Spicer LD. NMR studies of structure, hydrogen exchange, and main-chain dynamics in a disrupted-core mutant of thioredoxin. Protein Sci 1996;5:2552–2565.
62. Rader SD, Agard DA. Conformational substates in enzyme mechanism: the 120 K structure of α-lytic protease at 1.5 Å resolution. Protein Sci 1997;6:1375–1386.
63. Kraulis PK. MOLSCRIPT: a program to produce both detailed and schematic plots of protein structures. J Appl Crystallogr 1991;24: 946–950.